Generation of Reactive Species in Water Film Dielectric Barrier Discharges Sustained in Argon, Helium, Air, Oxygen and Nitrogen

Soheila Mohades¹, Amanda M. Lietz^{2,3} and Mark J. Kushner^{1,4}

- ¹ University of Michigan, Department of Electrical Engineering and Computer Science,1301 Beal Ave., Ann Arbor, MI 48109-2122 USA, soheila.mohades@gmail.com, mjkush@umich.edu
- ² University of Michigan, Department of Nuclear Engineering and Radiological Sciences,1301 Beal Ave., Ann Arbor, MI 48109-2122 USA, lietz@umich.edu
- Ourrent address: Sandia National Laboratories, 1515 Eubank Blvd. Albuquerque, NM 87123, USA
- ⁴ Author to whom correspondence should be addressed.

Abstract

Activation of liquids with atmospheric pressure plasmas is being investigated for environmental and biomedical applications. When activating the liquid using gas plasma produced species (as opposed to plasmas sustained in the liquid), a rate limiting step is transport of these species into the liquid. To first order, the efficiency of activating the liquid is improved by increasing the ratio of the surface area of the water in contact with the plasma compared to its volume – often called the surface-to-volume ratio (SVR). Maximizing the SVR then motivates the plasma treatment of thin films of liquids. In this paper, results are discussed from a computational investigation using a global model of atmospheric pressure plasma treatment of thin water films by a dielectric barrier discharge (DBD) sustained in different gases (Ar, He, air, N₂, O₂). The densities of reactive species in the plasma activated water (PAW) are evaluated. The residence time of the water in contact with the plasma is increased by recirculating the PAW in plasma reactor. Longer lived species such as H₂O_{2aq} and NO₃ and accumulate over time (aq denotes an aqueous species). DBDs sustained in Ar and He are the most efficient at producing H₂O_{2aq}, DBDs sustained in argon produces the largest density of NO_{3 aq} with the lowest pH, and discharges sustained in O₂ and air produce the highest densities of O_{3aq}. Comparisons to experiments by others show agreement in the trends in densities in PAW including O_{3aq}, OH_{aq}, H₂O_{2aq} and NO₃ aq, and highlight the importance of controlling desolvation of species from the activated water.

I. Introduction

Low-temperature atmospheric-pressure plasmas (APPs) are being investigated in applications from material processing to biomedicine and agriculture. The common interest in many of these applications is the interaction of APPs with liquids to activate or produce reactive species in the liquid. Plasma activation of liquid can be facilitated with the plasma in or in contact with the liquid which generally falls into three categories: (1) discharges sustained inside the liquid [1,2], (2) discharges in the gas phase inside the liquid, such as plasmas in bubbles [3,4], or (3) plasmas in gas in contact with liquid [5]. In the last approach, dielectric barrier discharges (DBDs), jets, corona, or gliding arcs have been investigated as a means to transfer plasma activated species into the liquid, which affects not only their chemical reactivity but also their conductivity and acidity.

The transport of gas phase species into the liquid is optimized by maximizing the surface area in contact with the plasma. With the goal of activating the volume of the liquid, the process is typically optimized by increasing the surface-to-volume ratios (SVR) of the surface receiving plasma activated species and the volume of liquid being activated. A reactor with a thin water film takes advantage of a high SVR and is therefore frequently studied in the water decontamination applications. The interface is the most activated layer where the decomposition of pollutant occurs. In a thin liquid film, the diffusion of pollutant to the activated interface occurs more rapidly due to the larger gradient, while also risking desolvation of those species as well.

In plasmas sustained in air, or having oxygen and nitrogen impurities, reactive oxygen species (ROS) and reactive nitrogen species (RNS) that are generated in the plasma transport to the surface of and solvate into the liquid. Although short lived aqueous species such as hydroxyl (OH_{aq}) are important in many applications, aqueous species such as hydrogen peroxide (H_2O_{2aq}) , nitrate (NO_{3aq}) and ozone (O_{3aq}) are often the end products of plasma activation of water due to their longer lifetimes and are effective in antibacterial applications [6-8].

Plasma based water decontamination has been investigated for a wide range of contaminants including dyes and organic compounds such as methylene blue and phenol [9,10]. Malik [11] described different plasma reactors and their energy efficiency for water purification applications, and suggested that pulse powered reactors operating on liquid sprays are the most energy efficient for producing plasma activated water (PAW). Foster [12] reviewed the progresses and needs in plasma-based water treatment as well as the technical challenges to scale-up and im-

plementation. Plasma remediation of hazardous chemicals in water such as dioxin, PCP, and TNT has been demonstrated. For example, DBDs have been shown to be effective in destruction of dioxin-like compounds – a highly toxic and environmentally persistent pollutant – due to the efficient production of UV radiation, solvated electrons, and OH radicals [13]. OH is a strong oxidant which reacts with most organics and several inorganic compounds and plays an important role in the removal of pollutants in water treatment applications [14].

With the goal of maximizing the efficiency of activating water by increasing the SVR, systems have been investigated where the APP contacts a circulating thin water film, typically covering one of the electrodes. The thin film has a large SVR while circulating the water enables buildup of long lived species in the water. Ognier *et al.* [15] experimentally investigated DBD treatment of a thin water film (0.14 mm thick) to remove acetic acid, phenol and heptanol. Results of a computational fluid dynamic model indicated that the mixing in the liquid film due to interfacial momentum transfer between gas and liquid can accelerate mass transfer of contaminants from the liquid bulk toward the interface and destruction of pollutants [15]. Andre *et al.* investigated a DC discharge in which plasma was ignited in air between two films of flowing tap water [16,17].

Kuraica *et al.* developed a DBD reactor with a circulating water film flowing over the dielectric surfaces of the coaxial system [18]. The discharge was sustained between the inner dielectric-covered electrode and the water-covered dielectric of the inner electrode operating in air, N₂, O₂, Ar and He. This *falling water DBD* (FW-DBD) reactor was used to investigate water purification and removal of pollutants such as phenol [19], arsenic [20], textile dyes [21] and gas phase pollutant such as NO_x and SO₂ [22]. For example, with a FW-DBD operating in air at 115 W, a 6 min plasma treatment of water resulted in significant removal of 2-chlorophenol (91%), 4-chlorophenol (85%) and 2,6-dichlorophenol (65%) [23]. The ability to customize the type and ratio of reactive species in these systems using different feed gases is attractive to target specific pollutants or destruction of organisms [24]. For example, OH and H₂O₂ are typically thought of as being the major biocidal components. However, measurement of gas phase and dissolved ozone in an indirect DBD sustained in air indicated a relatively high concentrations of O₃ (below about 0.2 W cm⁻²) and that 5 s of plasma treatment resulted in a completely *E. coli* bacteria inactivation [25]. The ability to selectively choose the active species would be an advantage.

In this paper, we report on results of a computational investigation using a global model,

of a low frequency *falling water* DBD reactor patterned after the work of Kovačević *et al.* [18] operating at atmospheric pressure in argon, helium, air, oxygen, and nitrogen, with trace air and water impurities. PAW is circulated through the reactor (that is, any volume of water sees several transits through the discharge) to better emulate the experiment and to evaluate ROS and RNS accumulation by increasing the residence time. The gas and liquid phase chemical reaction mechanisms will be discussed, with liquid phase densities compared to experiments for validation.

We found that FW-DBDs sustained in argon are the most efficient gas in the production of hydrogen peroxide in gas and water, generating 0.23 mM of H₂O₂ over 10 cycles of treating the PAW in agreement with experiments [18]. (M is moles/liter.) Production of gas phase hydroxyl is highest in argon plasma; however, the highest solvated hydroxyl density occurs with air plasmas, while the highest solvated ozone density occurs when operating the FW-DBD in the oxygen. Being short lived, the residual density of these OH and OHaq does not increase with the re-circulation. The density of HO₂ in argon and helium plasmas is several factors higher than in oxygen and air plasma due to the relative abundance of H atoms. Air plasma is the most efficient gas in the production of gas phase NO₂ and N₂O as well as ONOOH_{aq} in PAW. In all gases, density of NO_{3aq} increases linearly with re-circulation and the highest concentration was found in plasma sustained in argon (1.2 mM) followed by air (0.45 mM). With the presence of RNS, nitrate is the major contributor to the acidity of PAW therefore, the lowest pH was obtained in argon followed by air. Results from the model agree systematically and quantitatively with experiments for all species except for O_{3aq}. For O_{3aq}, agreement is systematic but not quantitative, a result that is attributed to desolvation of O_{3aq} during the afterglow. These results emphasize the importance of controlling desolvation from PAW.

The model used in the investigation is described in Sec. II followed by discussion of our computational scaling of FW-DBDs sustained in Ar He, air, O₂ and N₂ in Sec. III. The recirculation of PAW is discussed in Sec. IV. Concluding remarks are in Sec. V.

II. Description of the Model and Reactor Geometry

The model used in this investigation is a 0-dimensional global simulation, GlobalKin, which includes gas flow, transport of plasma activated species to-and-from the plasma-liquid interface and in-liquid reactions. The model is essentially the same as describe in detail in Ref.

[26] and so will be discussed only briefly here. GlobalKin consists of a set of rate equations whose integration provides densities of species in the gas and liquid phases as a function of time or, in plug-flow mode, as a function of position. The average electron energy in the gas phase plasma is obtained from an electron energy conservation equation. Electron impact rate coefficients and transport coefficients are obtained from solutions of Boltzmann's equation for the electron energy distribution, processed into a periodically updated look-up table as function of electron temperature.

The transport of species between the gas and liquid are limited by Henry's law equilibrium for the neutral species, while ions and photons from the gas phase can directly enter into the liquid. By definition, at Henry's law equilibrium the density of a gas dissolved in a liquid is proportional to the density of that species in the gas phase. At equilibrium, the liquid is saturated with the gas phase species. In the model, if the liquid is under-saturated for a particular species based on the Henry's law constant, transport of that gas phase species is allowed into the liquid. If the liquid is super-saturated (that is, the in-liquid density exceeds that at equilibrium), the net transport of the species is from the liquid to the gas. For instance, species with a small Henry's law constant saturate quickly in the liquid and its aqueous counterpart has a lower density. Species having a large Henry's law constant may never be saturated in the liquid, and continue to flow from the gas into the liquid.

The full reaction mechanism contains 98 gas phase, 92 liquid phase species and approximately 2070 gas and liquid phase reactions. The mechanism includes the species associated with He, Ar and humid air plasmas interacting with water. The gas phase reaction mechanism was adapted from Van Gaens *et al.* [27] for argon-humid air mixtures at atmospheric pressure. Extension to He-humid air and interactions with liquid water are based on the mechanism used by Lietz *et al.* [26], Tian *et al.* [28], and Norberg [29]. The mechanism only includes small water cluster ions $[O_2^+(H_2O), H^+(H_2O)_2, \text{ and } H_2O^+(H_2O)]$ in the gas phase. The additional reactions added to the mechanisms are discussed in the Supplementary Information. The interaction of ions and excited states of He with liquid H₂O was estimated based on the branching ratios from the gas phase analogues [28,30]. Henry's law constants used in this work are in Table 1.

A schematic of the FW-DBD reactor used in this investigation, shown in Fig. 1, based on the experiments of Kovačević *et al.* [18]. In the experiment, water was pumped from a reservoir, flowed along the dielectric covered surface of the inner electrode, returned to the reservoir and

then re-circulated through the reactor for ten cycles. The FW-DBD is a concentric 1 cm long cylindrical reactor with two dielectric covered electrodes with inner and outer radii of 10 mm and 14.5 mm making for a 4.5 mm discharge gap. The water film on the inner electrode is 0.22 mm thick. The reactor operates at atmospheric pressure and room temperature. Conceptually, the global model is applied to a control volume or plug of liquid film plus the surrounding gas. The control volume resides in the plasma for 1.56 s to match the experiment. Five gas mixtures were examined – Ar, He, air, O₂ and N₂, with a flow rate of 5 slm. Since the experiment was operated without special vacuum equipment, air and H₂O impurities were added to the gas mixtures in the simulation. Evaporation from water layer is included in this model and reaches to a steady state of 2.5% humidity for all gases. The liquid is pure water with 8.93 ppm (based on molecular densities) dissolved N₂ and 4.81 ppm dissolved O₂, the equilibrium values with air. The diffusion length in the gas phase is $d/\pi = 1.36$ mm, where d is the width of the discharge gap. When including the saturated water vapor, the air gas mixture is $N_2/O_2/H_2O = 77.5/20/2.5$, and helium and argon mixtures are 96.5% pure with 3.5% added humid air impurities (N₂/O₂/H₂O = 0.8/0.2/2.5). Accordingly, the mole fractions of N_2 in the nitrogen plasma is 97.3% and O_2 in oxygen plasma is 96.7%. CO₂ as an air impurity was not included in the reaction mechanism.

In this model, we specified power deposition as a function of time as a 21 W triangular pulse with 40 ns duration at 600 Hz (1.66 ms inter-pulse period). The applied power peaks at the calculated magnitude to provide the measured average power of 21 W to all gases. In the experiment, a sinusoidal voltage at a frequency of 300 Hz was used. Our choice of 600 Hz, 40 ns power pulses acknowledges that experimentally discharge pulses are produced at least twice per cycle, and that the individual discharges are typically only tens of ns long. The experimental dissipated powers were 60, 41, 32, 21 and 16 W for the discharges in air, nitrogen, oxygen, argon and helium respectively, to provide empirically stable operation with the water film and uniformly distribution of microdischarges along the reactor. Therefore, the power in argon matches that of the experiment. Applied power in the model extends for roughly 1500 pulses (2.5 s) after which the system evolves during the afterglow for 10 s (12.5 s total). To simulate PAW recirculation, the final density of gas and liquid species at 12.5 s are used as the initial inputs to simulate the next cycle. The recirculation was conducted 10 times, with each cycle beginning with the final density from the previous cycle at the same operating conditions. By holding the inner and outer electrodes at 300 K, there is no significant gas heating in the base case.

III. Plasma Activation of Water Film

A. Plasma Properties Operating in Different Gases

The FW-DBD was operated in the 5 gas mixtures (Ar, He, air, O₂, N₂) with an input power of 21 W. The electron density (ne) and temperature (Te) are shown in Fig. 2 for the first pulse. A triangular power is applied over 40 ns with the maximum power density of 13.4 kWcm⁻³ at 20 ns. The initial pre-pulse electron density was 1×10^8 cm⁻³. In all gases, the density of electrons increases during the pulse rise time, peaks shortly after 20 ns at maximum power and decays with a distinctive rate for each gas composition. As the electron density avalanches during the power rise time, the plasma conductivity increases and so the E/N of plasma decreases which then leads to a reduction in T_e. For instance, in helium T_e decreases from 8.8 eV to 3.7 eV at the maximum power deposition. The maximum n_e occurs in helium, 3.4×10^{12} cm⁻³, followed by the argon plasma with $9.5 \times 10^{11} \text{ cm}^{-3}$. The lowest n_e is in nitrogen plasmas, with a peak at 1.0×10^{11} cm⁻³. With power being specified, the electron density is in large part determined by the power dissipation per electron for collisions with the feedstock gases (with impurities) at a given T_e. Power dissipation per electron is lowest in He requiring a higher electron density to dissipate the peak power. Power dissipation per electron is highest in N₂ requiring a lower electron density to dissipate the peak power. Experimental measurements in APP showed that at a constant applied voltage, current and ne are higher in Ar than in He which agrees with the lowest dissipated power in He [31,32]. Te in all gases sharply decreases during the power fall time so that the power-dissipation per electron decreases.

The decay of electron density shows two distinct rates in these gases, fast (order of 10s of ns) and slow decay (up to hundreds of μ s). In helium, argon, and nitrogen the electron loss processes are dominated by electron-ion recombination with the rare gas dimer ions and N_2 molecular ions, and dissociative attachment to the water vapor. For air and oxygen plasmas, attachment to O_2 can be a dominant electron loss process and is largely responsible for the more rapid reduction in electron density for those mixtures. Electron attachment to O_2 in APPs follows two pathways, 2-body dissociative attachment producing O^- which has a threshold energy of 3.64 eV and 3-body attachment to form O_2^- with thermal electrons. The rate coefficient for 3-body electron attachments to O_2 increases with decreasing T_e (< 1 eV). Therefore, 3-body attachment is the dominant pathway for electron losses during the power-down portion of the pulse and afterglow when T_e is not high enough for a dissociative attachment. For discharge pulses after the

first, the buildup of RONS (reactive oxygen and nitrogen species) such as O_3 , N_2O and O_2^* (dominated $O_2(^1\Delta)$) can introduce additional attachment pathways. O_2 is an electronegative gas so density of electron reduces quickly during the fall time. T_e remains relatively high (3.1 eV) up to the end of the power pulse in the oxygen and air plasmas, resulting in 2-body attachment being the dominant electron loss process and n_e decreasing rapidly up to the end of the pulse. In argon, helium, and N_2 plasmas, T_e decreases during the power fall time to below the threshold for 2-body attachment threshold (down to around 1 eV). With the O_2 density being lower and relying on 3-body attachment and dissociative recombination, the electron decay time increases to hundreds of ns to microseconds.

Densities of short lived ions originating from humid mixtures (with impurities) for Ar, He, air, O_2 , and N_2 plasmas for the 1st pulse are shown in Fig. 3, and for the last, 1500th pulse after a 2.5 s plasma discharge are shown in Fig. 4. H_2O^+ is generally the dominant positive ion during the discharge for mixtures other than air and O_2 (that is, for mixtures in which O_2 is an impurity) and O_2^+ is the dominant ion in the air and O_2 mixtures. These trends result from these ions having the lowest ionization potential and a reasonably large mole fraction of their parent neutral molecule, and so can be produced by rapid charge exchange. The main source of H_2O^+ at this point is electron impact ionization of H_2O , charge exchange from ions having larger ionization potentials (HeH⁺, He⁺, He₂⁺ in helium; Ar⁺ and Ar₂⁺ in argon, and N_2^+ in N_2) and Penning ionization from the rare gas excited states. With these processes, H_2O^+ is the first ion to rise in density in Ar, He and N_2 plasmas. Those mixtures with large mole fractions of O_2 have O_2^+ as the ion with the initially rising density.

The density of O^- is limited to the pulse duration in O_2 and air indicating that the main pathway to its formation is the 2-body dissociative attachment (with a threshold energy of 3.6 eV). The 3-body attachments at low T_e in other gases results in later formation of O_2^- . Formation of O_2^- is dominantly through the charge exchange reaction of O_2 or O_3 with O^- or through 3-body attachment to O_2 :

$$O^- + O_2 \to O_2^- + O$$
, (1a)

$$e + O_2 + M \rightarrow O_2^- + M$$
, (1b)

$$O^- + O_3 \to O_2^- + O_2$$
. (1c)

The maximum density of O2 occurs in oxygen plasmas in which it is the most abundant ion. In

oxygen and air plasmas, O_2^- density raises and saturates soon after the power terminates with the dominant pathway being charge exchange reactions (equation 1a). However, in other gases (Ar, He, and N_2), O_2^- peaks hundreds of ns later when T_e is below 0.04 eV and so the 3-body reaction is the primary pathway. These trends for the density of O_2^- match well with time history of n_e and T_e for each gas.

Short lived species including ions and vibrationally and electronically excited species, are formed and consumed on a pulse-to-pulse basis by electron impact and are quenched or consumed by reactions prior to the next pulse. O_3^- is formed relatively late through the pulsing after the density of O_3 has achieved a reasonably large value. The lowest density of O_3^- is in nitrogen and highest density in oxygen due to higher density of O_2^- and O_3^- and larger densities of O_3 . The major pathways to O_3^- formation are:

$$O^- + O_2 + M \to O_3^- + M$$
, (2a)

$$O^- + O_3 \to O_3^- + O$$
, (2b)

$$O_2^- + O_3 \to O_3^- + O_2$$
. (2c)

In oxygen and air plasmas, O_3^- decays with two rates. Initially during early pulses, 2-body reactions (Eq. 2b and 2c) contribute to O_3^- formation. However, at later times, 3 body processes form O_3^- (Eq. 2a) and extends its lifetime to hundreds of μ s. Although, over 1500 pulses, O_3 accumulates in the plasma, resulting in direct charge exchange from O_3^- and O_2^- to O_3^- being the dominant source of O_3^- in oxygen and air plasmas.

The density of OH⁻ is higher in helium and argon plasmas and is formed at the beginning of the discharge by dissociative attachment to H_2O ($e+H_2O \rightarrow OH^- + H$). This reaction forming OH⁻ has a high threshold energy (4.5 eV) and so has a higher rate coefficient in Ar and He due to the larger T_e during the plasma avalanche. The density of OH⁻ peaks at the peak of the input power and gradually decays, producing the highest density in He discharges. OH⁻ develops relatively later in oxygen and air due to the lower T_e , decay earlier in oxygen (a few μ s) due to charge exchange to form O_3^- .

The densities of O_2^+ , H_2O^+ , and O^- generally do not change with successive pulsing while densities and lifetime of ions such as O_2^- , O_3^- , and OH^- do change over pulsing. The relatively constant densities of O_2^+ , H_2O^+ , and O^- are a consequence of both their production and quenching being from reactions with species that are initially in the gas mixtures. The changes

in densities of O_2^- , O_3^- , and OH^- suggest the formation and quenching reactions for these ions are sensitive to the accumulation of products on a pulse-to-pulse basis. For instance, in plasmas sustained in helium and argon, over the 1500 pulses the lifetime of O_2^- decreases by a factor of about 10 and the density of O_3^- increases by a factor of 2 due to the accumulation of O_3 (Eq. 2b and 2c). In air, O_2 , and O_2 plasmas, the lifetime of OH^- decreases significantly with pulsing, a decrease that is more pronounced in O_2 which can be due to the charge exchange reaction with O_3 .

B. ROS and RNS in the Gas Phase

The water film thickness is 0.22 mm with 2.5 s residence time per pass through the reactor and total plasma treatment time of 25 s over ten cycles. In this section formation of RONS in gas and water over one cycle (pass) will be discussed -2.5 s of plasma exposure followed by a 10 s afterglow. Densities of neutral ROS and RNS in gas phase are shown in Figs. 5 and 6 respectively for each gas. With the multiple pulses, transient species such as O, OH, HO₂, H, N, and NO are produced and consumed from pulse-to-pulse to generate more stable species that approach a quasi-steady state. The relatively low frequency, 600 Hz, can work in favor of solvation and reactions in liquid phase when the diffusion time of the gas phase species is smaller than the inter-pulse period. If a gas phase species is likely to react with a product species in the gas phase (e.g., OH reacting with OH to form H_2O_2), having a long interpulse period enables the OH to solvate before encountering a newly generated density of OH in the gas phase produced by the next pulse. Lietz et al. [26] reported that the increase in pulse frequency in DBD plasmas decreases the density of most RONS in the liquid due to their likelihood to react with other RONS in the gas phase before solvating. The exceptions were O_{3aq} and HNO_{3aq} whose gas phase precursors are the end product of reactions in the gas phase, and so benefit from the higher repetition rate. The dominant neutral product in helium and argon plasmas is H₂, but in air, oxygen, and nitrogen plasmas O₃ is the dominant gas phase product. These species also have low Henry's law constants and accumulate in the gas phase rather than solvating.

With all gas mixtures being humid, decomposition of water generates OH, H and O through electron impact dissociation of water (dominantly by $e+H_2O \rightarrow O+2H+e$ and $e+H_2O \rightarrow OH+H+e$) or dissociative recombination of H_2O^+ or H_3O^+ . The larger densities of H_2O^+ in argon and helium plasmas produce higher densities of OH and O radicals through the

dissociative recombination process. OH is produced and consumed on a pulse-to-pulse basis with the loss being dominated by reactions which form H_2O_2 .

$$OH + OH \rightarrow H_2O_2$$
, $(k = 1.7 \times 10^{-11} \,\text{cm}^3 \text{s}^{-1})$, (3a)

$$H + HO_2 \rightarrow H_2O_2$$
, $(k = 3 \times 10^{-11} \,\text{cm}^3 \text{s}^{-1})$, (3b)

$$HO_2 + HO_2 \rightarrow H_2O_2 + O_2$$
, $(k = 2.2 \times 10^{-13} \text{ cm}^3 \text{s}^{-1} E_a = -600 \text{ K})$. (3c)

(The rate coefficients, k, are for a gas temperature of 300 K with units of cm³ s⁻¹ (1 cm³ s⁻¹ = 6.02×10^{20} M⁻¹ s⁻¹) unless otherwise noted.) Apart from electron impact dissociation of H₂O, Penning ionization and dissociative charge exchange also contribute to OH formation in ground and excited states in helium and argon plasmas,

$$Ar_2^+ + H_2O \rightarrow ArH^+ + OH + Ar , \qquad (4a)$$

$$He_{2}^{+} + H_{2}O \rightarrow OH(A) + HeH^{+} + He,$$
 (4b)

$$He^+ + H_2O \rightarrow H^+ + OH + He$$
. (4c)

Measurements using laser induced fluorescence (LIF) in a helium pulsed filamentary discharge showed that OH is mainly produced by charge transfer reactions to form H_2O^+ followed by electron–water ion recombination [33]. The high energy of He excited states can produce Penning ionization in O_2 and N_2 which results in a higher density of O_2^+ and N_2^+ . For instance, density of O_2^+ is one order of magnitude higher in helium than argon plasmas due to these Penning processes,

$$He^* + O_2[N_2] \to He + O_2^+[N_2^+] + e$$
 (5)

The high reactivity and short lifetime of OH limit the diffusion of OH into a water layer. H_2O_2 is a more stable ROS that also has the highest density in argon plasmas $(4 \times 10^{14} \text{ cm}^{-3})$ due to higher density of OH and HO_2 . H_2O_2 quickly reaches a steady state (in less than 1 s) as do its reactants (i.e., OH and HO_2). The densities of H_2O_2 and OH are lower in air and nitrogen plasmas 10^{12} - 10^{13} cm⁻³, due to the lower rates of dissociation of H_2O_2 , and lower rates of H abstraction from H_2O by O atoms. The initial decrease in H_2O_2 density on successive pulsing is due to the initial depletion in OH density. In all gases H_2O_2 is quickly depleted during afterglow–faster than the pump exhaust, due to solvation into the liquid and dissociation reactions such as $O + H_2O_2 \rightarrow H_2O + O_2$ with timescales of seconds.

H atoms are the other by-products of H₂O dissociation, which then react to form H₂ (

The largest production of O_3 is in air and oxygen plasmas due to the higher O_2 densities. The major contribution to production of O_3 , the reaction $O + O_2 + M \rightarrow O_3 + M$, directly depends on production of O atoms. As shown in Fig. 5(d) and (c), the highest O atom density is in oxygen (5 × 10¹⁴ cm⁻³) and air plasmas (8 × 10¹³ cm⁻³). Spectroscopy of the FW-DBD also indicated strong emission spectra of atomic O in the oxygen plasma [18].

Electron impact dissociation of O_2 and dissociative quenching of $N_2(A)$ by O_2 are the major pathways to form O atoms. The higher O and O_2 densities in air and oxygen plasmas yield more O_3 formation. The O_3 density in the gas phase reaches 6×10^{16} cm⁻³ in the oxygen plasma, which is more than 2 orders of magnitude higher than in helium and argon. The density of O_3 accumulates over pulsing in O_2 , N_2 , and air plasmas while the density of O_3 quickly saturates in He and Ar. It is known that humidity in a plasma reactor decreases the density of O_3 . The presence of water vapor in a FW-DBD is inevitable due to the evaporation (physical and thermal) from water. For instance, the O_3 density dropped by a factor of 4 in gas phase by flowing the water film through the reactor [18]. The evolution of short and long lived species during the last three pulses and afterglow in the argon plasma are shown in Fig. 5(f). The long lived species such as H_2O_2 and O_3 accumulate over pulsing. The densities of H, O and OH rise and fall on a pulse-to-pulse basis due to formation and consumption through each pulse. For example, the rapid decline in the density of O atoms is dominantly due to ozone formation. (The transient in H density occurs over a period of 1.5 - 2 μ s, and is not resolved in the figure.) Density of NO as an intermediate and less reactive species fluctuates nominally.

Densities of RNS in the gas phase after once cycle of plasma treatment are shown in Fig.

6 for argon, helium, air, oxygen and nitrogen plasmas including 2.5 s discharge and 10 s afterglow. Electron impact dissociation of N_2 (threshold energy of 12.25 eV) forms atomic nitrogen which initiates a sequence of reactions with N as pathways to RNS formation. Further RNS including N_xO_y and HNO_x (acids) are created at a slower rate during the afterglow. The dominant RNS is HNO_3 in helium and argon while the dominant RNS is N_2O in air, oxygen, and nitrogen plasmas. The higher rate of OH production in Ar and He plasmas contribute to acid formation whereas the higher rate of O production in air, oxygen and, to some degree, N_2 plasmas favor nitrogen oxides. The highest production of N atoms is in argon. Apart from electron impact dissociation, the chemical quenching of argon by N_2 , $[Ar^* + N_2 \rightarrow Ar + N + N]$ yield more atomic nitrogen.

The trend in NO formation is different for each gas as NO has several production and consumption pathways by being the precursor of many reactions. For instance, in argon and nitrogen plasma NO saturates quickly without significant accumulation while it builds up gradually in helium (more sources of NO). In air and oxygen, the production and consumption of NO occurs in a more pronounced manner from pulse-to-pulse. The density of NO is higher in argon and helium plasmas, around 1×10^{13} cm⁻³ because the higher production of OH contributes to more NO formation through $OH + N \rightarrow H + NO$ ($k = 4.7 \times 10^{-11}$ cm⁻³). On the other hand, NO has the lowest density in oxygen, 1×10^{11} cm⁻³, which is due to the low production of N which only slowly produces NO by reactions such as $O_2 + N \rightarrow NO + O$ ($k = 3.3 \times 10^{-12}$, $E_a = 31,500$ K). Another rapid source of NO production is through excited state N₂, $O + N_2^* \rightarrow NO + N^*$ ($k = 7 \times 10^{-12}$ cm⁻³) that is more dominant in air and oxygen plasma due to higher density of O.

In air, NO rapidly reacts to produce NO_2 . Air plasma is the most efficient gas in the production of NO_2 as well as N_2O . N_2O is less reactive in the gas phase and has a small Henry's law constant (solvation is a loss process to the gas phase species) and so it builds up over pulsing in the gas phase during 2.5 s of discharge. On the other hand, NO_2 generally saturates in the gas phase (with the exception of air) during pulsing and then increases in density in the afterglow (again air is the exception). NO_2 in the gas phase reaches to a steady state being the most stable RNS. By the end of the afterglow (12.5 s) NO_2 is around 1×10^{12} cm⁻³ in argon, helium, and air plasmas and an order of magnitude lower in oxygen and nitrogen plasmas.

NO₂ and NO₃ are short lived ions in the gas phase which are produced and consumed

from pulse-to-pulse. Both ions are formed over the course of multi-pulses through several pathways. The density of NO_3^- is higher than NO_2^- in nitrogen, air and oxygen plasmas while it is slightly lower in helium and argon plasma. NO_2^- is depleted with high O_3 densities by conversion to NO_3^- :

$$O_3 + NO_2^- \to NO_3^- + O_2$$
 (6)

The density of HNO₂ in air and oxygen plasmas is the same order of NO₂ while its density in helium, argon and nitrogen plasmas exceeds that of NO₂. In addition to reactions between NO and OH, HNO₂ is produced by associative charge exchange between $HNO_3 + NO_2^-$, and 3-body ion-ion recombination reaction, $OH^- + NO^+ + M \rightarrow HNO_2 + M$. The density of HNO_x is the highest in argon plasmas, 6×10^{14} cm⁻³, followed by helium, 3×10^{14} cm⁻³ and air 2×10^{14} cm⁻³. These trends are due to the higher densities of OH⁻ (Fig. 4a,b) and OH (Fig. 5a,b) in these plasmas. In nitrogen and oxygen plasmas the density of HNO_x is approximately 2×10^{13} cm⁻³. HNO₃ is the dominant HNO_x in all gases.

After 2.5 s of plasma discharge –slightly more than 1500 pulses–power is turned off and simulation of the afterglow continues for 10 s, which represents one cycle of plasma water film treatment. After the discharge is extinguished, electrons and gas phase ions recombine in tens of milliseconds. Distinct phases of decay during afterglow can be seen in Fig. 5 and 6. The density of short lived species such H, O, and N decrease immediately after the discharge, transient species such as OH, NO, and HNO $_x$ decay relatively fast with a timescale of hundreds of milliseconds while more stable species last longer in the gas phase during the afterglow. For the 10 s of afterglow, species are exhausted out of the reactor with the gas flow which leads to 3 orders of magnitude density reduction with the residence time of 1.6 s.

Another mechanism for loss of gas phase species is the diffusion and solvation onto the water layer. Although this process is always occurring, it is particularly important to densities of gas phase species during the afterglow when the production rate of reactive gas phase species is small. O₃, H₂, and N₂O are less reactive and quickly reach an equilibrium with their liquid counterparts due to their small Henry's law constants. Therefore, these species are pumped out of the reactor leading to around 3-log density reduction without further solvation into the water or dissociation into other species.

More reactive species have a shorter lifetime during afterglow as they undergo gas phase

reactions that accelerate their loss on shorter time scales than solvation onto water or flow out of the reactor. These species include H_2O_2 , HO_2 , HO_2 , HO_3 , and NO_3 . For instance, H_2O_2 loss is enhanced by dissociation reactions such as $OH + H_2O_2 \rightarrow H_2O + HO_2$ ($k = 4.53 \times 10^{-12}$ cm³ s⁻¹, $E_a = 289$ K) on the timescale of seconds which contributes to HO_2 formation. As shown in Fig. 5(a), after around 6 s (the time varies for each gas), H_2O_2 reaches a steady state (i.e. production equals loss). For HNO_2 and HNO_3 , loss processes have shorter times than the flow time. For these species, their large Henry's law constants accelerate their losses by solvation. (The liquid is not saturated and so solvation continues throughout the afterglow.) The density of NO_2 increases at the end of the discharge because its production rate is larger than its loss through the formation reactions 7(a-c) and its density remains unchanged during afterglow:

$$OH + NO_3 \rightarrow HO_2 + NO_2$$
, $(k = 2 \times 10^{-11} \text{ cm}^3 \text{s}^{-1})$ (7a)

$$HO_2 + NO_3 \rightarrow OH + NO_2 + O_2$$
, $(k = 4 \times 10^{-12} \text{ cm}^3 \text{s}^{-1})$ (7b)

$$HO_2 + NO \rightarrow OH + NO_2$$
, $(k = 3.6 \times 10^{-12} \text{ cm}^3 \text{s}^{-1}, E_a = 270 \text{ K})$. (7c)

C. ROS and RNS in the Liquid Phase

The density ROS and RNS in the water are shown in in Figs. 7 and 8 for each gas mixture. Aqueous species are denoted by the "aq" subscript. In our model, positive ions from the gas phase solvate in the water and undergo charge exchange to form $H_2O^+_{aq}$, in which $H_2O^+_{aq}$ quickly produces hydronium ($H_3O^+_{aq}$) and OH_{aq} by reactions with H_2O_{aq} . Water dissociation can occur by excitation transfer processes where excited states in the gas phase quench on the surface of the water, $M^* + H_2O_{aq} \rightarrow M_{aq} + H_{aq} + OH_{aq}$. Electrons diffusing into the water quickly solvate, and charge transfer with O_{2aq} to form $O_2^-_{aq}$. Neutral species can solvate from the gas phase into water until they reach the equilibrium density with their gas phase counterpart. In this global model, water is resembled as a well stirred liquid which does not resolve diffusion inside liquid. Consequently, it is possible to overestimate solvation for species with very small Henry's law constants. These species may, in fact, saturate at the surface of the liquid before transport deeper into the liquid, thereby reducing the solvation of gas phase species. With significant convection in the liquid (approaching the well-stirred reactor limit), the surface resident aqueous species are mixed into the volume faster than by diffusion alone.

OH is short lived in the gas phase as well as in liquid, and so the solvation of OH from

gas phase should be at the proximity of the gas-liquid interface. OH_{aq} is produced by several mechanisms, including solvation of OH from the gas phase, dissociative excitation of H₂O_{aq} by excited states and ions incident from the gas phase forming water ions. Virtually all ionization processes of H₂O_{aq} rapidly produce OH_{aq} through the formation of hydronium: $H_2O_{aq}^+ + H_2O_{aq} \rightarrow H_3O_{aq}^+ + OH_{aq}$. Reaction of O_{aq} with water produces OH_{aq} , $O_{aq} + H_2 O_{aq} \rightarrow 2OH_{aq}$ ($k = 2.2 \times 10^{-17} \text{ cm}^{-3} \text{s}^{-1}$) that contributes to OH_{aq} formation during afterglow, particularly in air and oxygen plasma which indicate slower trend in OH_{aq} decay. In addition, decomposition of peroxynitrous acid (ONOOH_{aq}) under acidic conditions yields OH_{aq}. The density of O_{aq} is higher with oxygen plasmas (1 × 10¹⁰ cm⁻³); 2 times higher than that with air plasmas, and more than 3 times that with argon plasmas. Premixed dimethyl sulfoxide DMSO in water was used in the experiments as a probe to quantitatively measure OH_{aq} [6,18]. Reaction of OH_{aq} with DMSO produces methane sulfinic acid (CH₃SOOH) and methyl radicals (CH₃*) that can be measured with chromatography. This measurement is akin to a titration experiment. The molarity of DMSO is chosen to be large enough so that OH_{aq} reacts with DMSO before reacting with other species. The final densities of the reaction products of OH_{aq} and DMSO are therefore an integral of all OH_{aq} produced in the system. Kovačević et al. reported that the highest production of OH_{aq} was obtained with oxygen plasmas and its inventory increases linearly with the residence time (number of PAW re-circulations). Since OH_{aq} is highly reactive, during pulsing in the absence of DMSO, its density is in a quasi-steady state - generated and consumed with each pulse. OH_{aq} is consumed and its density decreases continuously during the afterglow.

 H_2O_{2aq} is not as reactive as OH_{aq} due to lower oxidation potential and is one of the most stable ROS in water. Its contribution to water purification is then more indirectly through decomposition into OH_{aq} in which metallic catalysts such as Fe^{2+} , Cu^{2+} , and nano-TiO₂ are added in a solution to catalytically increase H_2O_{2aq} decomposition [24]. Two major pathways to H_2O_{2aq} are solvation of H_2O_2 (Henry's constant 1.92×10^6) from the gas phase or formation in the liquid through:

$$OH_{aa} + OH_{aa} \rightarrow H_2O_{2aa}, (k = 1.7 \times 10^{-11} \text{ cm}^3 \text{s}^{-1}).$$
 (8)

The density of H_2O_{2aq} increases during pulsing and slowly reaches its Henry's law equilibrium with the gas phase then remains unchanged during the afterglow. The most efficient plasma for H_2O_{2aq} production is sustained in argon, with the density of 5×10^{16} cm⁻³ at 10 s of

afterglow. In ascending order, helium and oxygen plasmas then produce the next highest densities of H₂O_{2aq}. These trends correlate well with the density of H₂O₂ in the gas phase suggesting that solvation can be the dominant pathway for the production of H₂O_{2aq} in this system. With helium plasmas, there is small decrease in the H₂O_{2aq} density during the afterglow which is due density of H₂ (see Fig. 5(b)) which dissociate $H_{2aq} + H_2 O_{2aq} \rightarrow H_{aq} + O H_{aq} + H_2 O_{aq}$. Another reaction that generates $H_2 O_2$ in PAW is the recombination of hydroperoxyl radicals as $HO_{2aq} + HO_{2aq} \rightarrow H_2O_{2aq} + O_{2aq}$. HO_{2aq} in the water is mostly solvated from the gas phase due to its high Henry's constant as so its density grows slowly. The solvated density of HO_{2aq} follows that of its gas phase partner producing the maximum aqueous density with argon plasmas ($1 \times 10^{14} \text{ cm}^{-3}$). The higher H_{aq} density with argon and helium plasmas (approximately 2 orders of magnitude higher than in other gases) produces higher densities of HO_{2aq} by the reaction $O_{2aq} + H_{aq} \rightarrow HO_{2aq}$. Although the minimum concentration of HO_{2aq} occurs in oxygen plasmas, the lowest gas phase density of HO₂ occurs with nitrogen plasmas.

Hydronium, $H_3O^+_{aq}$, is formed by the reactions of H^+_{aq} and $H_2O^+_{aq}$ with water, and by hydrolysis of HNO_{xaq} species. The density of $H_3O^+_{aq}$ increases over time, thereby decreasing the pH of the water. The highest density of $H_3O^+_{aq}$ and the lowest pH occurs with argon plasmas. Based solely on initial solvation of charge species, electron solvation dominantly produces O_{2aq}^- whereas positive ion solvation produces $H_3O^+_{aq}$. Therefore, a significant imbalance between O_{2aq}^- and $H_3O^+_{aq}$ would indicate production of $H_3O^+_{aq}$ by other processes. The major source of $H_3O^+_{aq}$ other than positive ion solvation is hydrolysis of HNO_x gas phase species, ultimately producing $H_3O^+_{aq}$, and $NO_3^-_{aq}$, and $NO_3^-_{aq}$.

In the falling water experiments, Kovačević *et al.* measured H_2O_{2aq} in both water and DMSO solutions, where in the latter OH_{aq} is scavenged by DMSO [18]. It was shown that there is no H_2O_{2aq} in DMSO solutions when treated by air, nitrogen, and argon plasmas which implies that the origin of H_2O_2 in its aqueous form is the through the $OH_{aq} + OH_{aq}$ reaction in these systems. In helium and oxygen plasmas, solvation from the gas phase was reported to be the main pathway by observing H_2O_{2aq} in DMSO solution [18]. Other studies have also reported that the scavenging of OH_{aq} resulted in a lower H_2O_{2aq} density, a measure of the contribution of OH_{aq} recombination pathway in the formation of hydrogen peroxide in Ref. [14]. In contrast, meas-

urement of OH_{aq} and H_2O_{2aq} in water treated by plasma jets suggests that H_2O_{2aq} was not formed in the liquid, but instead is formed in the gas phase and then solvates into the liquid [34]. However, the SVR in this FW-DBD system is significantly larger than plasma jets and the gas diffusion length to the liquid is shorter. These conditions may facilitate the solvation of more OH into the liquid which then contributes to in-liquid formation of H_2O_{2aq} . The difference between the solvated OH_{aq} for plasmas sustained in different gas mixture in this model is nominal compared to that of H_2O_{2aq} . For example, there is a factor of 15 difference between H_2O_{2aq} produced by argon and air plasmas at the end of the discharge.

Ozone densities in the gas phase are highly dependent on the O_2 density in the gas mixture and the dissipated power [35]. Results for gas phase ROS in Fig. 5 shows that the highest density of O_3 is in oxygen plasma followed by air. The density of solvated O_{3aq} produced by different plasmas closely follows its density in the gas phase. Other than solvation of O atoms followed by reaction with dissolved oxygen, there are few ways to produce O_{3aq} other than solvation of O_3 from the gas phase. The highest O_{3aq} density is produced by the oxygen plasma, being 2×10^{16} cm⁻³ by the end of the discharge. From high to low O_{3aq} densities, the rankings are air, nitrogen, helium, and argon plasmas. Kovačević *et al.* reported that aquoeus ozone densities were higher with oxygen plasma followed by air, which agrees with the results from this model [18]. However the magnitudes of O_{3aq} between this model and the experiment are quite different. These differences result from desolvation from the thin film in the model, whereas the experiment collects the activated liquid between cycles decreasing its SVR. These discrepencies will be discussed below.

These results confirm that solvation of O_3 from the gas into liquid is the dominant source of O_{3aq} for these conditions. O_{3aq} under basic conditions decomposes via a series of chain reactions and produces OH_{aq} radicals in water in which the presence of H_2O_{2aq} accelerate its decomposition via $2O_{3aq} + H_2O_{aq} + OH_{aq}^- \rightarrow OH_{aq} + HO_{2aq} + 2O_{2aq} + OH_{aq}^-$ and $O_{3aq} + H_2O_{2aq} + OH_{aq}^- \rightarrow OH_{aq} + HO_{2aq} + OH_{aq}^-$ [36]. The small Henry's constant of O_3 results in rapid saturation of the water as shown in Fig. 7 and limits its aqueous concentration. During the 10 s afterglow, the density of O_{3aq} decreases by 3 orders of magnitude in all gases due to the diffusion out of the water to remain in equilibrium with gas phase density, and consumption by reactions in the water such as $NO_{2aq}^- + O_{3aq} \rightarrow NO_{3aq}^- + O_{2aq}^-$. In the FW-DBD

system, the surface to volume ratio of the water is large and if the solvated species is oversaturated, the species can desolvate from the liquid into the gas. This effect is most severe for species having smaller Henry's law constants. The key to long term retention of O_{3aq} in such liquids is mixing into the volume of systems with small SVRs. It was shown that the antibacterial effect of PAW strongly depends on gas-liquid mixing following plasma treatment [25].

The dynamics of solvated ions are different with helium and argon plasmas compared to oxygen and air plasmas. As shown in Fig. 7, the densities of O_2^- and OH_{aq}^- , as well as HO_{2aq} , increase during the afterglow with air and oxygen plasmas. These densities decrease during the afterflow with argon and helium plasmas. With oxygen and air plasmas, O_2^- and quickly charge exchanges with the higher density of O_{3aq} to produce O_3^- and $(k = 2.66 \times 10^{-12} \text{ cm}^{-3} \text{ s}^{-1})$. Being highly reactive, the densities of O_3^- and rapidly decrease during the discharge and the afterglow in all gases. Reaction of O_3^- and with OH_{aq} results in the further increase in O_2^- and OH_{2aq}^- densities through the reaction OH_{2aq}^- and OH_{2aq}^-

$$O_{3ag}^{-} + OH_{ag} \rightarrow O_{2ag}^{-} + HO_{2ag},$$
 (9a)

$$O_{3aq}^- + H_3 O_{aq}^+ \to O_{2aq} + H_2 O_{aq} + O H_{aq}$$
 (9b)

HNO_x solvates into water from the gas phase during the afterglow. Due to its large Henry's constant, its rate of decay is larger than that of convective flow out of the reactor. HNO₃, with a Henry's law constant in excess of 10^6 does not equilibrate during the afterglow with a monontonically decreasing density. HNO₂, with h $\approx 10^3$ does begin to equilibrate with HNO_{2aq} during the discharge and afterglow. The densities of HNO_{2aq} ($pK_a = 3.4$) decrease due to hydrolysis reactions (equation 10a) during the afterglow to reach a steady state in argon, helium, and air plasmas. Stability of weak acids such as HNO_{2aq} is pH dependent in which it dissociates to its anionic form (NO_{2-aq}) when the pH is above its pK_a . So, the decay of HNO_{xaq} is faster in oxygen and nitrogen plasmas due to higher pH of PAW. Similarly, HNO_{3aq} is dissociated by the hydrolysis reaction (equation 10b) that accumulates the NO_{3-aq} which is the dominant nitrogen-based ion in our system while the NO_{2-aq} density is significantly lower. The highest density of gas phase HNO₃ occurs in argon plasmas, that results in the highest density of NO_{3-aq}, while nitrate is an order of magnitude lower in oxygen and nitrogen plasmas due to the lower

production of gas phase HNO_x . In our system, the products of HNO_{3aq} hydrolysis are the major source of acidification.

$$HNO_{2aq} + H_2O_{aq} \to NO_{2aq}^- + H_3O_{aq}^+,$$
 (10a)

$$HNO_{3ag} + H_2O_{ag} \to NO_{3ag}^- + H_3O_{ag}^+$$
 (10b)

Other sources of HNO_{xaq} are the acid formation reactions from N_xO_{yaq} ,

$$NO_{2ag} + NO_{2ag} + H_2O_{ag} \to HNO_{2ag} + HNO_{3ag},$$
 (11a)

$$NO_{aq} + NO_{2aq} + H_2O_{aq} \rightarrow HNO_{2aq} + HNO_{2aq},$$
 (11b)

$$NO_{2aq} + H_{aq} \rightarrow HNO_{2aq}$$
, (11c)

$$NO_{2aq} + OH_{aq} \rightarrow HNO_{3aq},$$
 (11d)

$$N_2O_{4aq} + H_2O_{aq} \rightarrow HNO_{3aq} + HNO_{2aq}. \tag{11e}$$

The density of NO_{2aq} , similar to that of ozone, quickly reaches the steady state with its counterpart in the gas phase. This equilibrium of NO_{2aq} helps maintain the density of HNO_{2aq} in spite of the latter's rapid hydrolysis.

Formation of ONOOH_{aq} ($pK_a = 6.8$) is pH dependant and is formed through different reactions including $NO_{2aq} + OH_{aq}$ and $N_2O_{5aq} + H_2O_{aq}$. The latter reaction has equal branchings to form HNO_{3aq} and ONOOH_{aq} [26]. The longevity of NO_{2aq} helps buoy its density. Its conjugate base, ONOO aq, quickly reverts back to ONOOHaq during pulsing and the afterglow as the pH drops below 6.8. Production of $ONOOH_{aq}$ is higher with air plasmas (1 \times 10¹⁵ cm⁻³) due to the higher and prolonged density of OH_{aq} and a high concentration of N₂O₅. Furthermore, the decay of ONOOH_{aq} (less in PAW produced by air plasmas than other gases) into NO_{3 aq}, OH_{aq}, and NO_{2aq} prolongs the lifetime of these species during afterglow. Chemical analysis of phenol in PAW by Lukes et al., and the formation of hydroxylated and nitrated products of phenol, indicated the decomposition of ONOOH_{aq} and post-discharge production of OH_{aq} and NO_{2aq} [36]. Peroxynitric acid (HO₂NO_{2aq}) is formed in the gas phase through 3-body reactions and solvates with a large Henry's law constant. Its density in the gas phase as well as in liquid is higher in air and argon plasmas. Although HO₂NO_{2aq} decays thermally to HO_{2aq} + NO_{2aq} and HNO_{2aq}, it is relatively stable in helium, argon, and air produced PAW up to 10s afterglow. The hydrolysis of HO_{2aq} ($pK_a = 4.8$), particularly in helium and argon produced PAW, contributes to further increase in the density $H_3O^+_{aq}$ and $O_2^-_{aq}$. HO_{2aq} also reacts with OH_{aq} to form O_{2aq} and H_2O_{aq} .

IV. Re-circulating PAW

To model the recirculation of the PAW, the densities after 12.5 s from all gas and liquid species were used as the input density for the simulation of the next cycle, and this plasma treatment was repeated for ten cycles as in the experiment. In the experiment, PAW was collected in a container at the end of one cycle and then was loaded again into the DBD reactor for the next rounds of plasma treatments. Therefore, the evolution of liquid phase species in the experiment can be affected by more complicated environmental factors such as mixing, exposure to the ambient air, and changes in the surface-to-volume ratios. In the model, the time interval between each re-circulation was estimated to be 10 s. During all of this time, the SVR was the same as during the plasma activation.

In the experiment, DMSO was added to the water prior to the plasma treatment. As a result, OH_{aq} was rapidly titrated out of the water, producing a time integrated value for OH_{aq} production. The rapid titration of OH_{aq} , decreases the rates of reactions that are initiated by OH_{aq} , To compare the computed densities of OH_{aq} with measurements [18] the computed density of OH_{aq} was integrated over the total time (12.5 s) of the process and multiplied by the lifetime of OH_{aq} in our system (3 ms) to compensate the quick reaction of OH_{aq} with the molecular probe (DMSO). The time integrated concentration of OH_{aq} is shown in Fig. 9 for the first cycle. The OH_{aq} production in water is approximately the same during all cycles, suggesting a linear growth over the 10 cycles of recirculation. The highest integrated density of OH_{aq} is in air plasma produced PAW (20 μ M) due to the decomposition of species such as peroxinitrous acid and ozone ($O_{3aq}^- + H_3 O_{aq}^+ \rightarrow O_{2aq} + OH_{aq} + H_2 O_{aq}$). Considering a linear growth over 10 cycles and multiplying the data in Fig. 9, the density of OH_{aq} in our model is in agreement with the concentration, \sim 200 μ M, after the last cycle measured in the experiment. The density of OH_{aq} measured in the experiment was approximately 100 μ M in nitrogen, argon, and helium. The lowest integrated OH_{aq} density as shown in Fig. 9 is with the argon plasma as 5 μ M after one cycle.

Densities of H_2O_{2aq} in PAW produced by at the end of each cycle (12.5 s) are shown in Fig. 10a. The highest density of H_2O_{2aq} occurs with argon plasmas (plotted on the right axis), 0.25 mM after the 10^{th} cycle, which correlates well with the experimental data. Kovačević *et al.* showed that the highest production rate of H_2O_{2aq} in water is in argon plasma and the highest concentration is around 0.6 mM after the 10^{th} cycle [18]. Both the simulation and the experiment

indicate that H_2O_{2aq} accumulates over recirculation though the trend is different for each gas. With argon, helium, and nitrogen plasmas, there are incremental increases in the density of H_2O_{2aq} with each cycle, whereas with air and oxygen plasmas H_2O_{2aq} reaches a near steady state. According to the experiment, the lowest density of H_2O_{2aq} was obtained with oxygen and nitrogen plasmas while the density of H_2O_{2aq} was a factor of 3 higher with air plasma. As shown in Fig. 5, production of H_2O_2 in the gas phase during the discharge is also lower in air and nitrogen plasmas, which correlates well with its solvated counterpart suggesting solvation is the dominant pathway.

Densities of O_{3aq} at the end of the afterglow for each cycle are shown in Fig. 10(b). The concentration of O_{3aq} is approximately 21 nM and 12 nM when using oxygen and air plasmas, respectively, higher than in other gases. The density of O_{3aq} is lower by 2 orders of magnitude when using helium and argon plasma. There is no significant increment in O_{3aq} density with recirculation. These trends are attributed to the gas phase density of O_3 in this system reaching a steady state over the course of plasma pulses and O_{3aq} saturating by having small Henry's constant. Therefore, the concentration of O_{3aq} will not further increases with increasing the residence time or cycles. The lower concentrations of O_{3aq} when using He, Ar and N_2 plasmas is a consequence of the only source of oxygen being either impurities or dissociation of water vapor. The predicted densities of O_{3aq} for each gas correlates well with the results of the experiment – the highest O_{3aq} occurs with oxygen plasmas, followed by air and nitrogen plasmas.

Having reproduced trends of the experiments, the predicted concentrations of O_{3aq} presented in Fig. 10(b) are significantly lower than the experimental measurements. The differences can be attributed to the rapid loss of O_{3aq} in our model due to desolvation during the afterglow, as shown in Fig. 7. In the model, the thin-film nature of the plasma-water system is retained during the afterglow between plasma treatment cycles. With gas phase O_3 convected away from the liquid during the afterglow, the Henry's law equilibrium concentration of O_{3aq} also decreases. In the experiment, mixing, collection of the water into a volume having a smaller surface-to-volume ratio, and environmental factors can reduce the desolvation rate of O_{3aq} resulting in retaining a higher concentration of dissolved ozone between cycles.

With these considerations, the predicted densities of O_{3aq} at the end of the plasma discharge (and before the rapid desolvation during the afterglow) are perhaps the better comparison to the experiment. The predicted O_{3aq} at the end of plasma pulsing in oxygen (the highest densi-

ty) is approximately 20 μ M while in the experiment the concentration was 8 μ M. For plasmas sustained in nitrogen, the experimental density of O_{3aq} is ~2 μ M which is underestimated by the simulation as 0.15 μ M. The concentrations of O_{3aq} for air plasmas is 5.2 μ M in the experiment and 12 μ M in the model. In the the experiment, the density of O_{3aq} for plasmas in helium fluctuates around 0.1 μ M without a significant increase in density with recirculation, similar to the simulation results which also records a concetration of 0.1 μ M. These comparisons between the experimental measurements of O_{3aq} and the simulation results at the end of the pulsing qualitatively agree, and emphasize the need to manage the desolvation of species from thin water films.

The accumulation of nitrate, NO₃ aq, in PAW for plasmas sustained in different gases at the end of each cycle (discharge and afterglow) is shown in Fig. 10(c). In all gases, the NO₃ aq density increases linearly with the cycles of recirculation (residence time). The highest predicted concentrations of nitrate 1.2 mM in argon and 0.45 mM in air plasmas. The lowest densities of nitrate are in oxygen and nitrogen plasmas 0.04 mM. In the experiment, the densities of NO₃ aq in descending order were in air (2.5 mM), nitrogen (0.64 mM), and argon (0.22 mM) plasmas, while the density was nominal in oxygen and helium plasmas. These comparisons are complicated by variations in power deposition in the experiment, while power was constant across gases in the model. When running isolated cases with powers aligned with the experiments, the predicted density of NO₃ aq is highest in air plasmas (instead of argon), as in the experiment.

Solvation of NO_x species from the gas and the dissociation of acids in the water generate $H_3O_{aq}^+$ and decrease the pH of the PAW. Since HNO_{3aq} is a strong acid its hydrolysis (forming NO_{3aq}^-) is the major source of $H_3O_{aq}^+$. Therefore, the trend of pH in PAW follows the NO_{3aq}^- density as shown in Fig. 10(d). The pH in a descending order at the last cycle is 4.4 in oxygen and nitrogen, 3.6 in helium, 3.3 in air, and 2.9 in argon plasmas. The lowest pH in experiments was in air plasmas followed by nitrogen. When running powers identical to the experiments, the predicted pH is lowest for air plasmas.

V. Concluding Remarks

Production of PAW (plasma activated water) depends not only on the formation of gas phase precursors but also their transport and subsequent solvation into the water. A

computational investigation was performed of the formation of PAW in a flowing water dielectric barrier discharge (FW-DBD) in which a thin film of water is treated through serveral cycles while varying the feedstock gas (Ar, He, N₂, O₂, air) [18]. In each case, the feedstock gases become saturated with water vapor, and so precursor formation was in part determined by the reactions of the plasma activated feedstock gases with the water vapor. For example, the most efficient gases for OH production in gas phase were Ar and He, in part due to these interactions.

Although OH_{aq} is probably the most important oxidant in water treatment, it has a short lifetime in water, being produced and consumed during each discharge pulse and each cycle. The major product of OH_{aq} reactions, H_2O_{2aq} , is more stable and accumulates during the early cycles of cyclic treatment of PAW in the FW-DBD, with the highest production rate using argon. Prolonged densities of OH_{aq} result from in liquid reactions such as O_3^- and $ONOOH_{aq}$. Nitrate $(NO_3^-$ aq), produced dominantly by hydrolysis of HNO_x gas phase species, accumulates with succuessive cycles, the the largest densities being with Ar and air discharges, leading to these systems also being the most acidic to the co-production of H_3O^+ aq during the hydrolysis.

In general, the trends in the computed results for components in the PAW as a function of gas mixture aligned with experiments by Kovačević et al. [18], which lends credance to the calculations. The differences can in large part be attributed to the use of a global model for a geometrically complex system and uncertainties in power deposition. The exception to this agreement is in the measured and computed values of O_{3aq}, and the source of that disagreement is a major lesson of this work. In both experiment and computations, the concentrations of O_{3aq} saturated, a consequence of the low Henry's law constant of O3. However, the predicted densities of O_{3aq} at the end of after cycles were significantly below those of the experiment. The explanation is likely due to the manner in which the PAW was treated period plasma cycles. In the computations, the system was maintained in a thin-film configuration with a large surface-tovolume ratio (SVR), which enabled the O_{3aq} to desolvate. In the experiment, the collection and recirculation of the PAW produce mixing and resulted in a smaller SVR which reduced the rate of de-solvation of O_{3aq} . When comparing the post-plasma, saturated concentrations of O_{3aq} prior to desolvation, the agreement between calculations and experiments was reasonable. These results emphasize the need to actively manage the PAW to prevent (or enhance) the rate desolvation of species.

Modeling the many thousands of pulses and tens of seconds of processing time for five gas mixtures was a computationally intensive task, which would be beyond the current capabilities of the 2-dimensional or 3-dimensional models required to address, in detail, a geometrically complex system. Questions posed by a referee in this regard include whether such modeling can be predictive? The direct answer is that global modeling can be predictive, as demonstrated here, in a semi-quantitative way. However, as the geometric complexity of a system increases, the expectations should decrease that global modeling can provide a side-by-side quantitative representation of the experiment. The value of global modeling in this regard is in emphasizing important mechanisms and trends.

Acknowledgements

This work was supported by the National Science Foundation (PHY-1902878). This material was also based upon work supported by the U.S. Department of Energy, Office of Sciences Fusion Energy Sciences under award numbers DE-SC000319 and DE-SC0020232. This paper describes objective technical results and analysis. Any subjective views or opinions that might be expressed in the paper do not necessarily represent the views of the U.S. Department of Energy or the United States Government. The authors would like to thank Vesna V. Kovačević, Bratislav M. Obradović, and Milorad M. Kuraica for valuable insights to their experiments.

References

- [1] A. Starikovskiy, Y. Yang, Y. I. Cho, and A. Fridman, *Plasma Sources Sci. Technol.* **20**, 24003 (2011).
- [2] A. Yamatake, D. M. Angeloni, S. E. Dickson, M. B. Emelko, K. Yasuoka, and J.-S. Chang, *Jpn. J. Appl. Phys.* **45**, 8298 (2006).
- [3] R. Burlica, K.-Y. Shih, and B. R. Locke, *Ind. Eng. Chem. Res.* 49, 6342 (2010).
- [4] B. Pongrác, H. H. Kim, M. Janda, V. Martišovitš, and Z. Machala, J. Phys. D. Appl. Phys. 47, 315202 (2014).
- [5] S. Iseki et al., Appl. Phys. Lett. 100, 113702 (2012).
- [6] M. Sahni and B. R. Locke, *Ind. Eng. Chem. Res.* 45, 5819, (2006).
- [7] M. J. Traylor et al., J. Phys. D Appl. Phys. 44, 472001 (2011).
- [8] D. R. Grymonpré, W. C. Finney, R. J. Clark, and B. R. Locke, *Ind. Eng. Chem. Res.* 42, 5117 (2003).
- [9] H. A. and K. K. and S. Hamaguchi, Plasma Sources Sci. Technol. 17, 25006, (2008).
- [10] N. Sano et al., Ind. Eng. Chem. Res. 41, 5906 (2002).
- [11] M. A. Malik, *Plasma Chem. Plasma Process.* **30,** 21 (2010).
- [12] J. E. Foster, *Phys. Plasmas*, **24**, 55501 (2017).
- [13] C. Hung, S. H. Chang, K. H. Chi, and M. B. Chang, "J. Hazard. Mater. 182, 246 (2010).
- [14] J. Franclemont and S. M. Thagard, *Plasma Chem. Plasma Process.* **34**, 705 (2014).
- [15] S. Ognier, D. Iya-sou, C. Fourmond, and S. Cavadias, *Plasma Chem. Plasma Process.* **29**, 261 (2009).
- [16] Andre et al., J. Phys. D. Appl. Phys. **35**, 1846, (2002).
- [17] Andre, Y. A. Barinov, G. Faure, and S. M. Shkol'nik, *J. Phys. D. Appl. Phys.* 44, 375202, (2011).
- [18] V. V Kovačević, B. Dojčinović, M. Jović, G. M. Roglić, B. M. Obradović, and M. M. Kuraica, J. Phys. D. Appl. Phys. **50**, 155205 (2017).
- [19] D. Manojlovic, D. R. Ostojic, B. M. Obradovic, M. M. Kuraica, V. D. Krsmanovic, and J. Puric, *Desalination* **213**, 116 (2007).
- [20] D. Manojlović et al., Vacuum 83, 142 (2008).
- [21] B. Dojčinović et al., J. Hazard. Mater. 192, 763 (2011).
- [22] B. M. Obradović, G. B. Sretenović, and M. M. Kuraica, *J. Hazard. Mater.* **185**, 1280 (2011).
- [23] B. Dojčinovića, D. Manojlovićb, G. M.Roglićb, B. M.Obradovićcd, M. M.Kuraicacd, and J. Purić, *Vacuum* **83**, 234 (2008).
- [24] Y. Cao, G. Qu, T. Li, N. Jiang and T. Wang, *Plasma Sci. Technol.* **20**, 103001 (2018).
- [25] M. J. Pavlovich, H-W. Chang, Y. sakiyama, D. S. Clark and D. B. Graves, J. Phys. D Appl. Phys. 46, 145202 (2013).
- [26] A. M. Lietz and M. J. Kushner, J. Phys. D. Appl. Phys. 49, 425204, (2016).
- [27] W. Van Gaens and A. Bogaerts, *Plasma Sources Sci. Technol.* 23, 35015 (2014).
- [28] W. Tian and M. J. Kushner, J. Phys. D. Appl. Phys. 47, 165201 (2014).

- [29] S. A. Norberg, Modeling Atmospheric Pressure Plasma Jets: Plasma Dynamics, Interaction with Dielectric Surfaces, Liquid Layers, and Cells. (Doctoral dissertation) 2015. http://hdl.handle.net/2027.42/113342
- [30] W. Tian, K. Tachibana and M. J. Kushner, J. Phys. D: Appl. Phys. 47, 055202 (2014).
- [31] S. Z. Li, J. P. Lim, J. G. Kang and H. S. Uhm, *Phys. Plasmas.* **13**, 093503 (2006).
- [32] H. Wang, R. J. Wandell and B. R. Locke, J. Phys. D: Appl. Phys. 51, 094002 (2018).
- [33] T. Verreycken, N. Sadeghi and P. J. Bruggeman, Plasma Sources Sci. Technol. 23, 045005 (2014).
- [34] G. Yury, D. O'Connell, and C. Victor, "Non-Thermal Plasma in Contact with Water: The Origin of Species," *Chem.Eur. J.* **22**, 3496 (2016)
- [35] B. Eliasson and U. Kogelschatz, IEEE Trans. Plasma Sci. 19, 309 (1991).
- [36] P. Lukes, E. Dolezalova, I. Sisrova and M. Clupek, Plasma Source Sci. Technol. 23, 015019 (2014).
- [35] R. Sander, Atmos. Chem. Phys. 15, 4399 (2015).

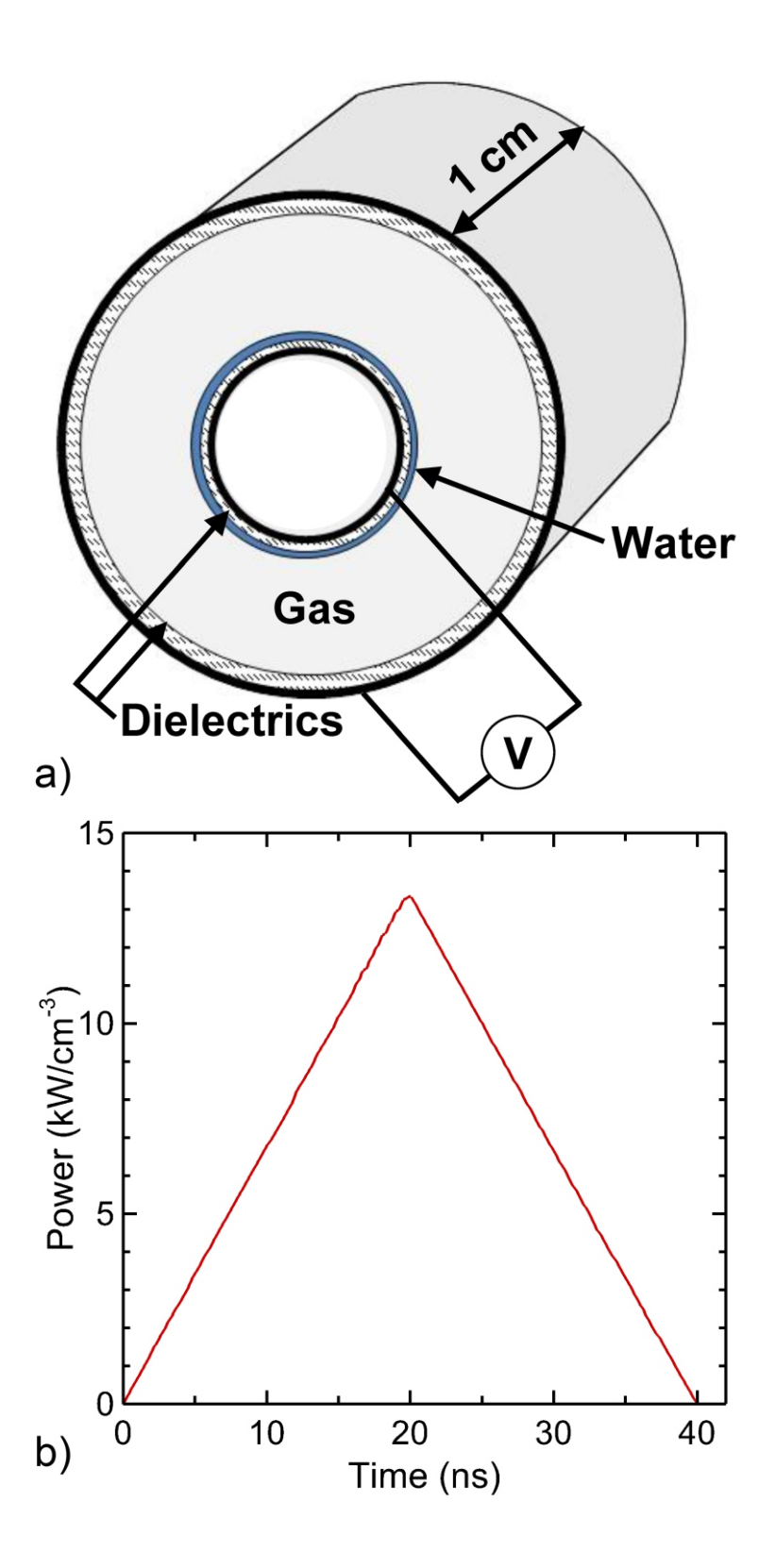
Table 1. Henry's Law Constants (Ref. [26])

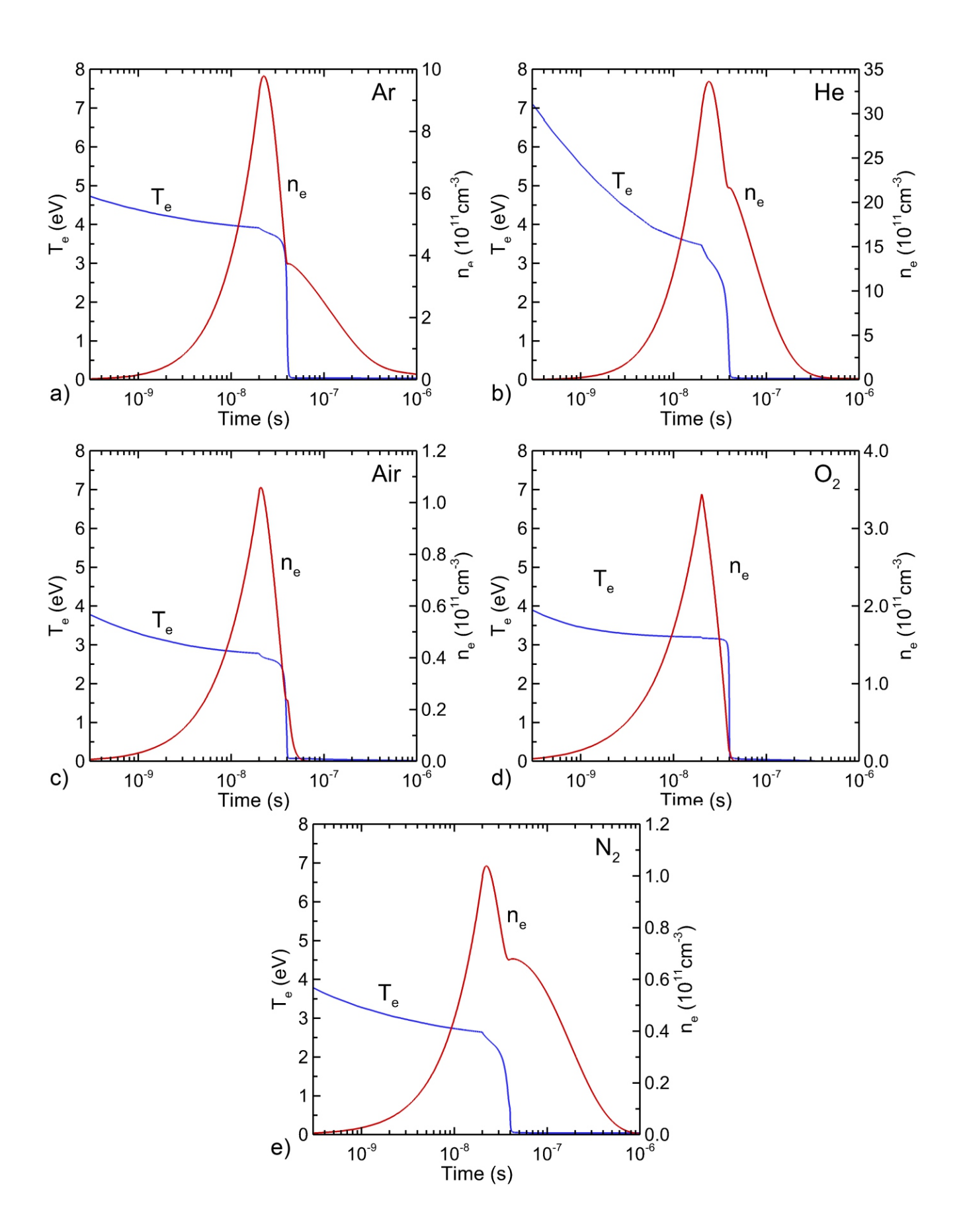
Species	h (unitless)	Note
H_2O_2	1.92×10^6	
HO_2	1.32×10^5	
ОН	6.20×10^{2}	
Н	6.48×10^{3}	
H_2	1.80×10^{-2}	
$O, O(^1D)$	1	a,b
O_2 , $O_2(v)$,	3.24×10^{-2}	a
$O_2(^1\Delta_g), O_2(^1\Sigma_u)$		а
O_3	3.00×10^{-1}	
$N_2, N_2(A^3\Sigma_u), N_2(v), N, N(^2D), N_2(a^{-1}\Sigma)$	1.60×10^{-2}	a
N_2O_3	6.00×10^{2}	
N_2O_4	3.69×10^{1}	
N_2O_5	4.85×10^{1}	
N_2O	5.99×10^{-1}	
HO_2NO_2	2.99×10^{5}	
NO	4.40×10^{-2}	
NO_2	2.80×10^{-1}	
NO_3	4.15×10^{1}	
HNO_2 , HNO	1.15×10^3	a
HNO ₃ , ONOOH	4.80×10^{6}	
NH	1.47×10^3	c

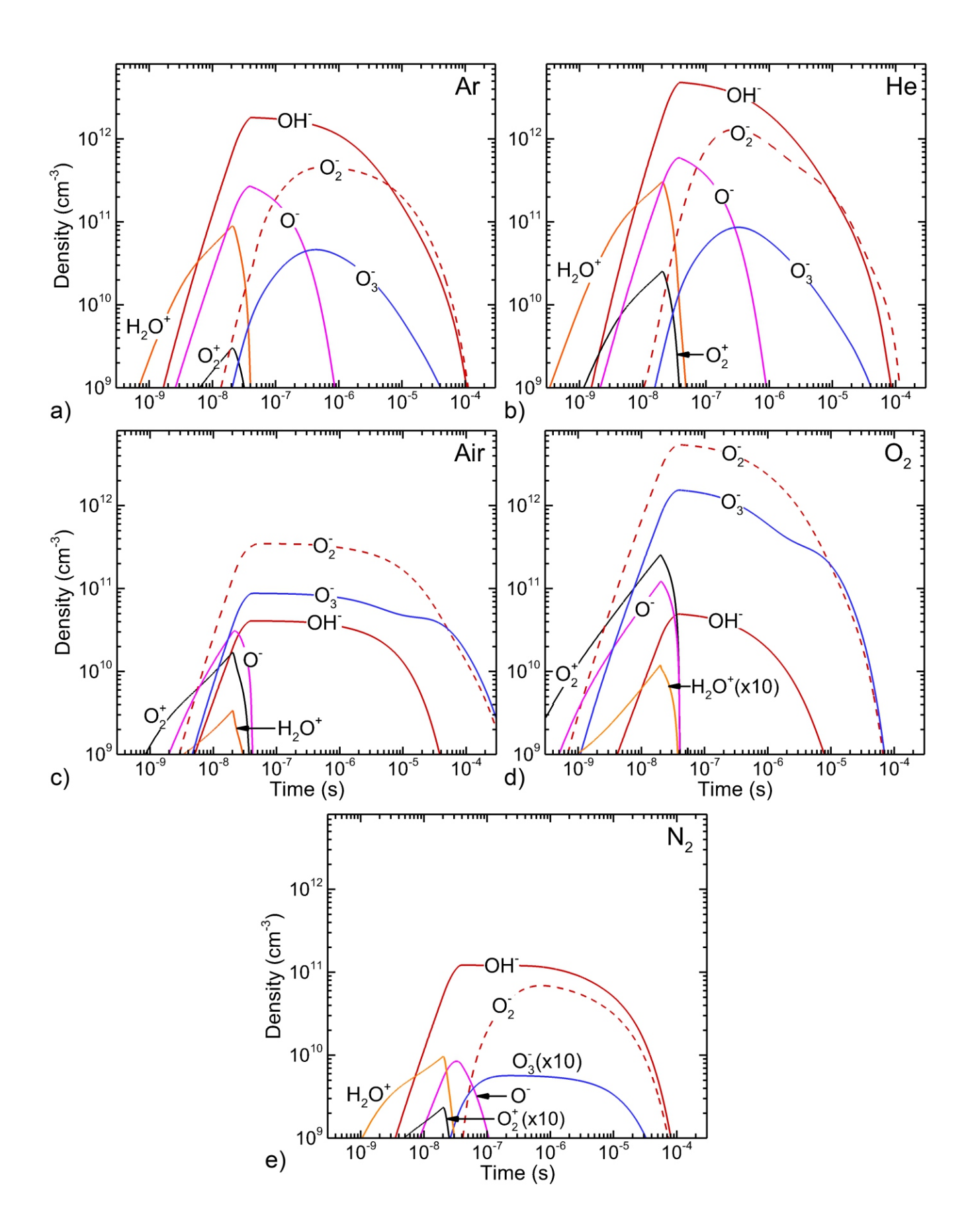
a) Value corresponds to the first species in the list. Other species were assumed to have the same Henry's law constant.
b) Approximated. Species reacts quickly in water and will not reach Henry's law saturation.
c) Approximated by analogy to NH₃.

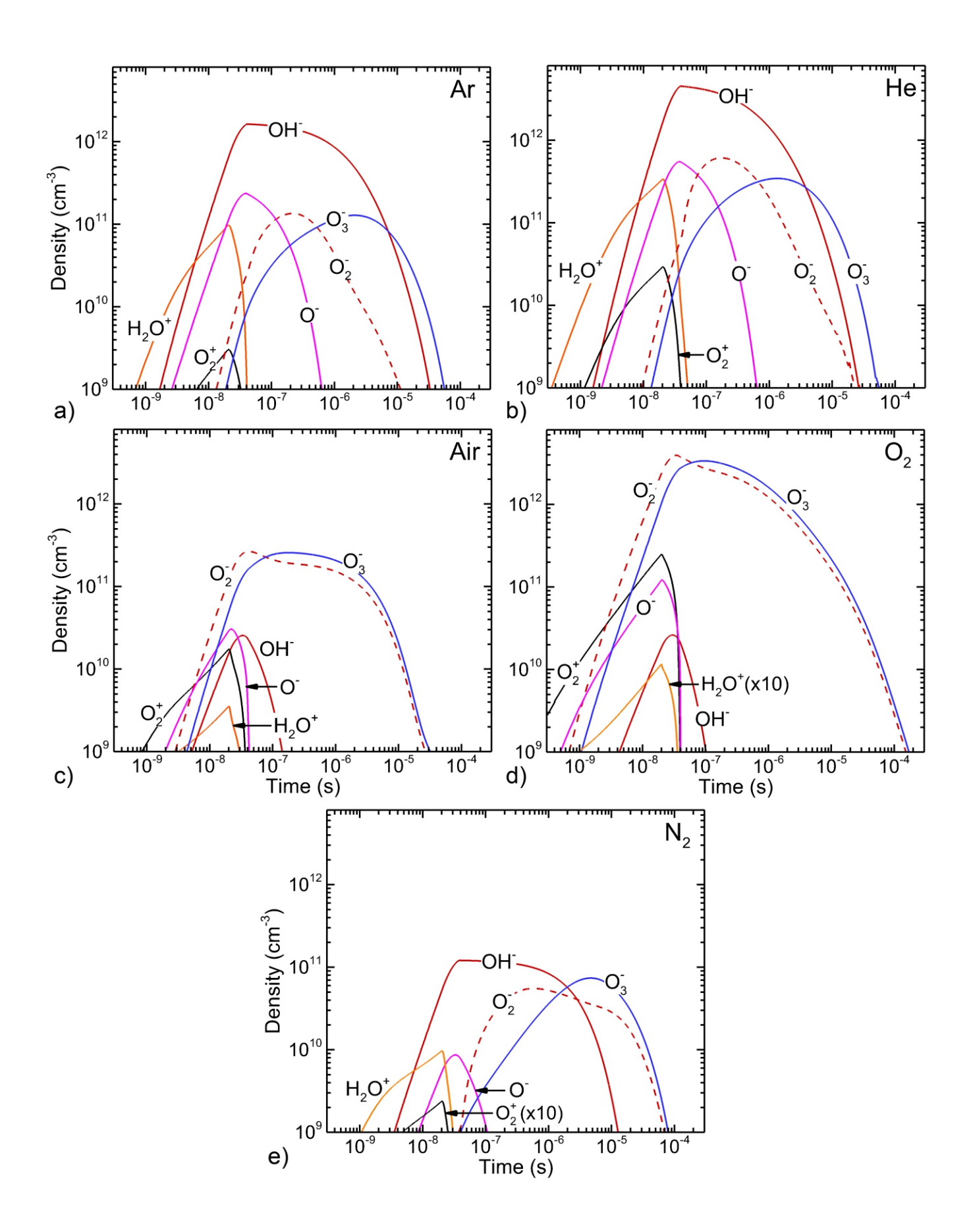
Figure Captions

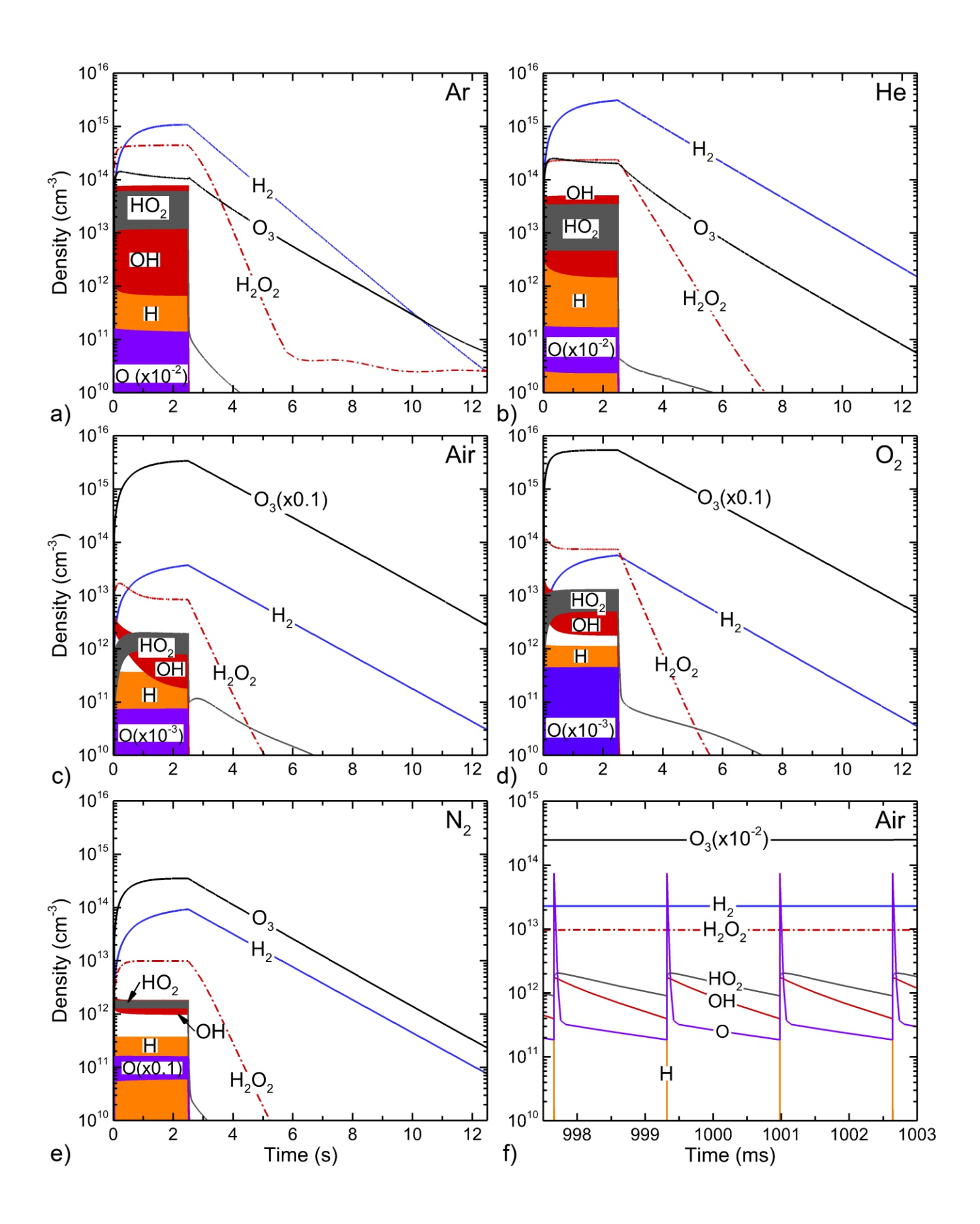
- 1. Operating schematic and conditions. a) Schematic of the flowing water DBD reactor. The DBD has an inner radius of 10 mm, outer radius of 14.5 mm and 4.5 mm gap. The water film is 0.22 mm thick. b) Power profile used in the model. This pulse is repeated at 600 Hz.
- Electron temperature and density during the discharge pulse for different feed gases. a) Ar,
 b) He, c) air, d) O₂ and e) N₂.
- 3. Density of gas phase ROS (reactive oxygen species) during the first discharge pulse of the first cycle for different feed gases. a) Ar, b) He, c) air, d) O₂ and e) N₂.
- 4. Density of gas phase ROS (reactive oxygen species) during the 1500th discharge pulse of the first cycle for different feed gases. a) Ar, b) He, c) air, d) O₂ and e) N₂.
- 5. Density of gas phase ROS (reactive oxygen species) during the first cycle (2.5 s of plasma exposure and 10 seconds of afterglow) for different feed gases. a) Ar, b) He, c) air, d) O₂ and e) N₂. f) ROS for an air feedstock are shown on an expanded time scale during the plasma period.
- 6. Density of gas phase RNS (reactive nitrogen species) during the first cycle (2.5 s of plasma exposure and 10 seconds of afterglow) for different feed gases. a) Ar, b) He, c) air, d) O₂ and e) N₂. f) RNS for an air feedstock are shown on an expanded time scale during the plasma period.
- 7. Density of liquid phase ROS (reactive oxygen species) during the first cycle (2.5 s of plasma exposure and 10 seconds of afterglow) for different feed gases. a) Ar, b) He, c) air, d) O₂ and e) N₂.
- 8. Density of liquid phase RNS (reactive nitrogen species) during the first cycle (2.5 s of plasma exposure and 10 seconds of afterglow) for different feed gases. a) Ar, b) He, c) air, d) O₂ and e) N₂.
- 9. Integrated production of aqueous OH_{aq} during the first cycle of 2.5 ms of plasma exposure and 10 s of afterglow. (M is moles/liter.)
- 10. Aqueous properties as function of number of cycles of processing with each cycle consisting of 2.5 s of plasma exposure and 10 seconds of afterglow for different feedstock gases. a) H₂O_{2aq}, b) O_{3aq}, c) NO_{3aq}. (M is moles/liter) and d) pH of the liquid.



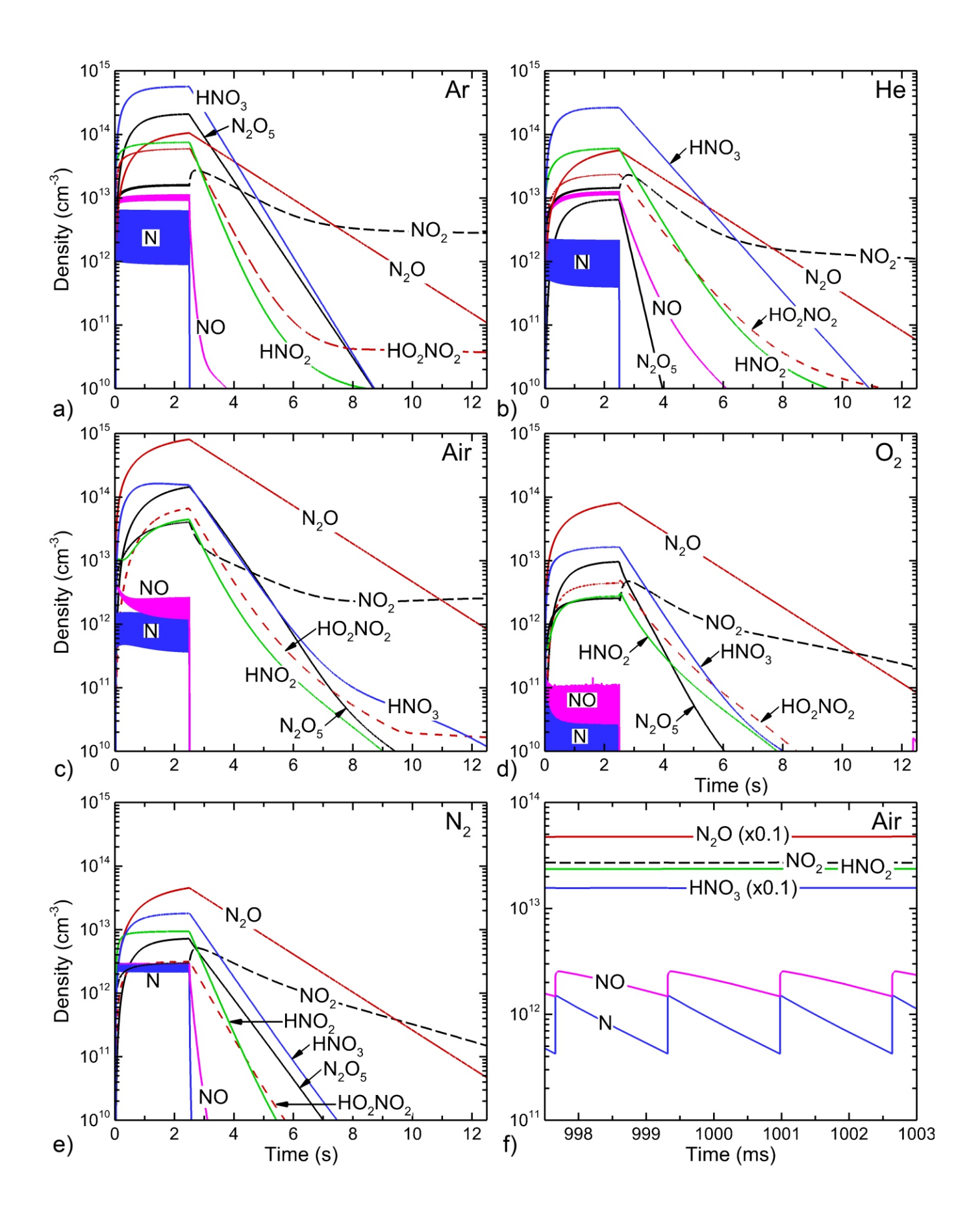




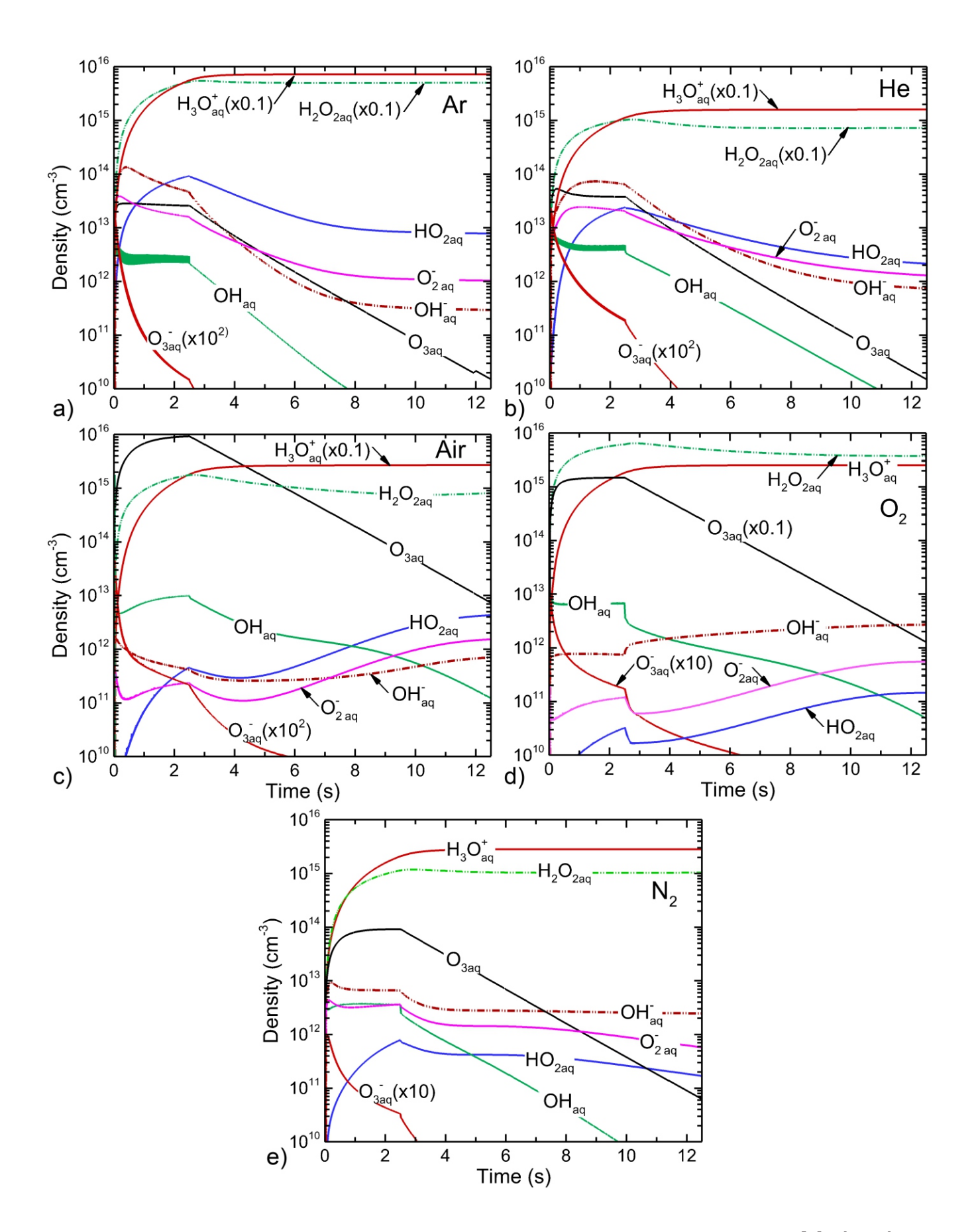




Mohades et al Fig 5 of 10



Mohades et al Fig 6 of 10



Mohades et al Fig 7 of 10

